Hyperconjugation |Hot Paper|

The Combination of Cross-Hyperconjugation and σ-Conjugation in 2,5-Oligosilanyl Substituted Siloles

Alexander Pöcheim,[a] Gül Altınbaş Özpınar,[b] Thomas Müller,*[b] Judith Baumgartner,*[a] and Christoph Marschner*[a]

Dedicated to Prof. Uwe Rosenthal, a fantastic chemist, a great man, and a dear friend, on the occasion of his 70th birthday

Abstract: Reaction of a 2,5-dilithiated silole with excess dichlorodimethylsilane gives the respective 2,5-bis(chlorodimethylsilyl) substituted silole. This compound can be converted to 2,5-bis(oligosilanyl) substituted siloles by addition of a suitable oligosilanide. In the UV spectra of the thus obtained compounds the lowest energy absorptions are bathochromically shifted compared to the absorptions of the two constituents, namely the 2,5-disilyl substituted silole and a trisilane. The bathochromic shift is interpreted as being caused by a mixed σ-conjugation/cross-hyperconjugation. This assumption is supported by TD-DFT calculations, which show a significant contribution from Si–Si bonds to the HOMO of the molecule.

Introduction

Much of contemporary organic material chemistry depends on conjugated molecules. Typically, this expression refers to organic π-conjugated compounds, where sp^2-hybridized carbon atoms in a co-planar arrangement lead to the formation of an extended π-system. Apart from plain π-conjugation of alternating multiple bonds, other types of conjugation are known such as that of cross-hyperconjugation[1,2] present in siloles and related molecules[3–7] and that of σ-conjugation, which is known for polysilanes and other catenated heavy group 14 elements (Figure 1).[3,8] It is also known that different types of conjugation can be combined, and phenyl substituted siloles and polysilanes can be considered as examples of mixed π-conjugation/cross-hyperconjugation and π-conjugation/σ-conjugation, respectively.[9–11] In the present study, we want to show that the combination of siloles as the prototypical examples of cross-hyperconjugated molecules and oligosilanes, representative of σ-conjugation, form systems of extended conjugation leading to altered optical absorption properties.

The discovery that siloles possess interesting electron and hole transporting properties[12,13] and the subsequent finding that some siloles exhibit the hitherto unknown phenomenon of aggregation-induced-emission (AIE),[14–16] established a reputation for these compounds as materials for numerous applications such as organic light emitting diodes, chemical sensors and biological probes.[16]

As a consequence, many differently substituted siloles were prepared and their photophysical and electronic properties studied. Since the desired AIE property is restricted to some structural requirement such as the presence of phenyl groups in 3,4-positions and rather rigid substituents in 2,5-positions, much research was devoted to this particular substitution pattern.[13]

From a theoretical point of view, siloles are interesting as they exhibit an unusual type of conjugation, namely cross-hyperconjugation or σ*–π*-conjugation.[17] Examples of the combination of silole cross-hyperconjugation with another form of

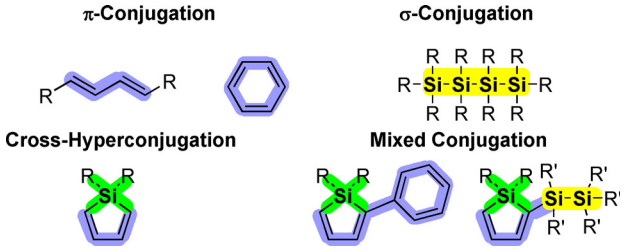

Figure 1. Three different types of electron delocalization and two types of mixed conjugation: π-conjugation/cross-hyperconjugation and σ-conjugation/cross-hyperconjugation as addressed in the present study.

[a] A. Pöcheim, Dr. J. Baumgartner, Prof. Dr. C. Marschner
Institut für Anorganische Chemie, Technische Universität Graz
8010 Graz (Austria)
E-mail: baumgartner@tugraz.at
christoph.marschner@tugraz.at

[b] Dr. G. A. Özpınar, Prof. Dr. T. Müller
Institut für Chemie, Carl von Ossietzky Universität Oldenburg
26111 Oldenburg (Germany, European Union)
E-mail: thomas.mueller@uni-oldenburg.de

Supporting information and the ORCID identification number(s) for the author(s) of this article can be found under: https://doi.org/10.1002/chem.202003150.

conjugation, namely that of π-conjugation, are known, and even the combination of cross-hyperconjugation with σ-conjugation such as present in oligo- and polysilanes[8] has been studied. However, previous attempts have either concentrated on the preparation of oligo- or polysilanes consisting of silole units (i.e. poly-1,1-siloles)[18,19] and related germanium compounds[20] or on a polysilane in which a 1,1-silole unit is incorporated at every fifth position of a regular methylated polysilane, which was obtained by ring-opening polymerization of a tetraphenylsilole-spiro-[4.4]-octamethylcyclopentasilane.[21]

Our intention in the current study was to probe for mixed conjugation of a silole with σ-conjugated units attached to the 2- and 5-positions. For this reason, we decided to prepare and study a number of siloles with silyl or oligosilanyl groups in 2,5-positions.

Results and Discussion

Synthesis

Yamaguchi and Tamao's approach of using di(phenylalkynyl)silanes is well suited to introduce various substituents to the 2,5-positions of siloles.[22] Reduction with lithium naphthalenide gives the respective 2,5-dilithiosiloles. Further reaction with electrophiles provides access to various 2,5-disubstituted siloles. The installation of silyl groups into these positions is particularly facile as long as the groups are not too sterically encumbered. For the present study, we decided to use di(phenylalkynyl)silane **1**, bearing two methyl groups at silicon, as a starting material. Reductive cyclization with lithium naphthalenide was followed by reaction with excess dichlorodimethylsilane to the 2,5-chlorodimethylsilyl substituted silole **2** (Scheme 1). If chlorotrimethylsilane was used instead of dichlorodimethylsilane, the 2,5-bis(trimethylsilyl) substituted silole **4** was obtained (Scheme 1).

The chlorodimethylsilyl substituents of **2** provide the possibility to introduce oligosilanyl groups to the 2,5-positions. Reaction with potassium tris(trimethylsilyl)silanide[23,24] led to formation of the neopentasilanyl substituted silole **3** (Scheme 1). Compound **2** was also reacted with 1,1,4,4,4-pentakis(trimethylsilyl)tetramethyltetrasilanyl potassium[25] to yield compound **5** with attached oligosilanyl fragments containing linear hexasilane units (Scheme 1).

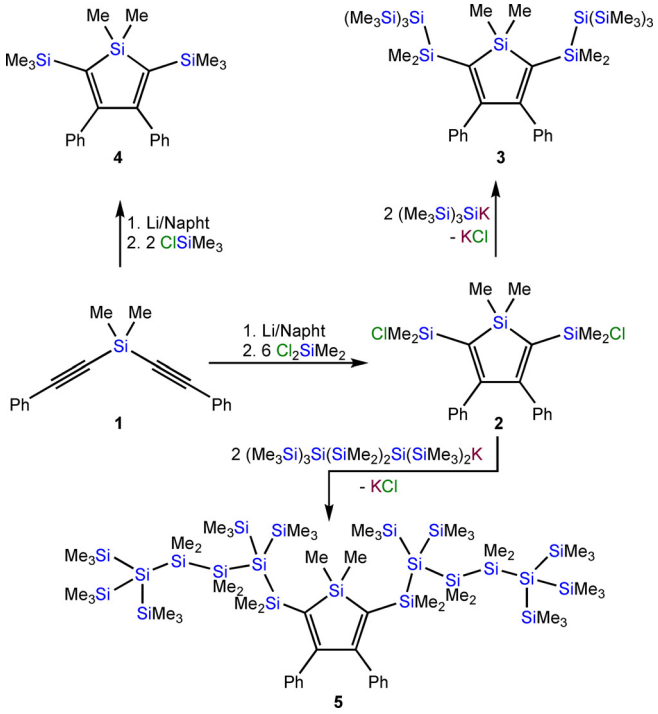

Scheme 1. Synthesis of a variety of 2,5-disilyl substituted siloles.

X-ray crystallography

Siloles **2**, **3**, and **4** were subjected to single-crystal X-ray diffraction analysis. The quality of the structure of the Me_2ClSi and Me_3Si substituted compounds **2** and **4**, both crystallizing in the monoclinic space group *C*2/*c*, is good and a discussion of structural parameters is possible. In contrast, the quality of the structure of the neopentasilanyl substituted compound **3**, crystallizing in the triclinic space group P-1, does not warrant a detailed discussion. This is in part caused by strong disorder in a tris(trimethylsilyl)silyl unit of one of the two crystallographic independent molecules in the asymmetric unit. Nevertheless, the principal constitution of neopentasilanyl substituted silole **3** could be established and in particular also some information on the conformational properties of the attached neopentasilanyl substituents can be gathered from the structure analysis. The structural parameters of the 3,4-diphenylsilole core which is shared by **2**, **3**, and **4** are fairly similar. There is clear localization of the 2,3- and 4,5-double bonds which exhibit CC-bond lengths close to 136 pm. It is somewhat surprising that the chloride atoms of the Me_2ClSi substituents of compound **2** (Figure 2) are not disordered over the three possible positions but are localized. This is unusual as the van der Waals radii of methyl groups and chlorides attached to silicon are fairly similar, which in the absence of any directing effects usually leads to disorder of the methyl and chloride substituents over all three positions. For silole **2** (Figure 2), the two Si–Cl bonds

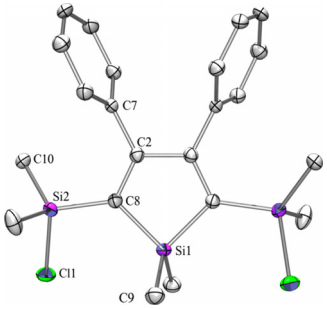

Figure 2. Molecular structure of **2** (thermal ellipsoid plot drawn at the 30% probability level). All hydrogen atoms are omitted for clarity (bond lengths in pm, angles in deg). Cl(1)–Si(2) 210.00(13), Si(2)–C(8) 185.6(3), Si(2)–C(10) 186.0(3), Si(1)–C(9) 186.9(3), Si(1)–C(8) 188.5(3), C(8)–C(2) 136.0(4), C(8)-Si(2)-C(10) 115.04(14), C(8)-Si(2)-Cl(1) 104.40(10), C(9)-Si(1)-C(9A) 111.0(2), C(9)-Si(1)-C(8) 110.40(14), C(2)-C(8)-Si(2) 124.3(2), C(2)-C(8)-Si(1) 106.2(2), Si(2)-C(8)-Si(1) 129.45(17).

(210 pm) are slightly out of the silole ring plane with chloride atoms pointing toward the silicon end of the silole ring but to different sides of the ring plane. This leads to two chlorodimethylsilyl groups positioned in a *trans*-diaxial arrangement.

For compound **3** (Figure 3), the tris(trimethylsilyl)silyl units of the neopentasilanyl substituents are oriented perpendicular to the ring plane. This suggests that this axial position is better suited for large substituents. A similar picture already emerged in the study related to 2,5-bis(dimethylphenylsilyl) substituted siloles,[26] where the phenyl groups occupied axial positions.

For compound **4** (Figure 4) the cell parameters are very similar to that of **2**. Again there is a clear localization of the 2,3- and 4,5-double bonds which exhibit C–C bond lengths of 135.2 pm and even the conformation of **4** is similar to that of **2** with the chloride atoms of **2** being replaced by methyl groups.

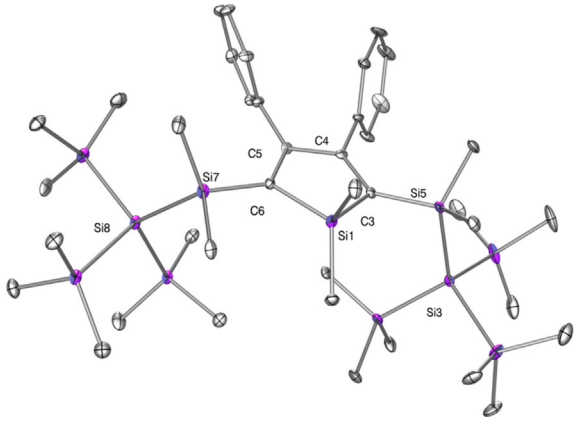

Figure 3. Molecular structure of **3** (one of two molecules in the asymmetric unit drawn, thermal ellipsoid plot drawn at the 30% probability level). All hydrogen atoms are omitted for clarity (bond lengths in pm, angles in deg). Si(1)–C(1) 187.1(6), Si(1)–C(2) 188.2(6), Si(1)–C(3) 188.5(6), Si(1)–C(6) 189.4(6), Si(3)–Si(5) 238.3(2), Si(5)–C(3) 187.0(6), Si(7)–C(6) 188.4(6), Si(7)–Si(8) 237.5(2), C(3)–C(4) 136.1(7), C(4)–C(5) 153.0(8), C(5)–C(6) 135.5(8), C(1)-Si(1)-C(2) 107.7(3), C(1)-Si(1)-C(3) 116.2(3), C(2)-Si(1)-C(3) 109.1(3), C(1)-Si(1)-C(6) 120.7(3), C(2)-Si(1)-C(6) 107.5(3), C(3)-Si(1)-C(6) 94.7(2), C(3)-Si(5)-Si(3) 113.28(18), C(6)-Si(7)-Si(8) 118.27(18), C(4)-C(3)-Si(5) 127.9(4), C(4)-C(3)-Si(1) 104.9(4), Si(5)-C(3)-Si(1) 126.3(3), C(3)-C(4)-C(5) 117.0(5), C(6)-C(5)-C(4) 117.7(5).

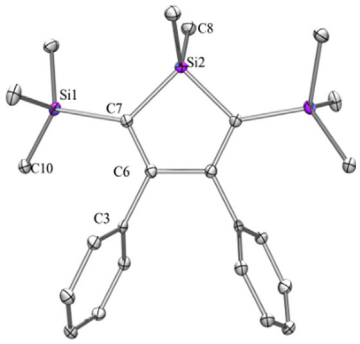

Figure 4. Molecular structure of **4** (thermal ellipsoid plot drawn at the 30% probability level). All hydrogen atoms are omitted for clarity (bond lengths in pm, angles in deg). Si(1)–C(7) 186.9(2), Si(1)–C(10) 187.0(2), Si(2)–C(7) 187.9(2), Si(2)–C(8) 186.8(2), C(7)–C(6) 135.2(2), C(6)–C(6A) 150.7(2), Si(1)-C(7)-Si(2) 127.94(9), C(7)-Si(2)-C(7A) 94.33(11), C(8)-Si(2)-C(8A) 108.7(1), C(7)-C(6)-C(3) 124.5(1).

Absorption spectroscopy

UV spectra of all described compounds were measured (Table 1, Figure 5) and several trends can be recognized from the data. For the 2,5-monosilylated compounds **2** and **4**, sharing the 1,1-dimethylated silole core, the absorption data are similar. Low energy bands at 300 nm and 301 nm, respectively, are close to that for 1,1,2,5-tetramethyl-3,4-diphenylsilole ($\lambda =$ 307 nm)[27,28] and 1,1-dimethyl-2,5-diethyl-3,4-diphenylsilole ($\lambda = 301$ nm)[27] indicating no immediate influence of the silyl group on the conjugated system. Compounds **3** and **5** with oligosilanyl substituents in the 2,5-positions of the silole ring show a distinct bathochromic shift of the low energy bands to 331 and 332 nm, respectively. For compound **5** a very strong additional band at 259 nm was observed.

1,1-Dimethyl-2,3,4,5-tetraphenylsilole ($\lambda = 361$ nm)[15] was assigned as an example for the combination of silole cross-hyperconjugation and phenyl π-conjugation. The bathochromic shift of compounds **3** and **5** compared to **2** and **4**, thus also might be an indication of some sort of mixed conjugation of the 1,1-dimethyl-3,4-diphenylsilole unit with the attached oligosilanyl groups. Neither the permethylated neopentasilane ($\lambda = 210$ nm)[29] nor 2,2,5,5-tetrakis(trimethylsilyl)decamethylhexasilane ($\lambda = 257$ nm)[30] are known to exhibit absorptions beyond 300 nm. The observed bathochromic shifts of the

Table 1. UV absorption data of compounds **2**–**5** with a 1,1-dimethyl-3,4-diphenyl silole core and $SiMe_2R$ groups in 2,5-positions.

Compound	λ [nm]	shoulder λ [nm]	ε [$M^{-1}cm^{-1}$]
2 (R = Cl)	260		7.1×10^3
	300		7.5×10^3
3 (R = $Si(SiMe_3)_3$)	286		5.3×10^3
	331		9.6×10^3
4 (R = Me)		230.0	11.1×10^3
		260.5	4.5×10^3
	301		5.2×10^3
5 (R = $Si(SiMe_3)_2(SiMe_2)_2Si(SiMe_3)_3$)	259		116×10^3
	332		14.5×10^3

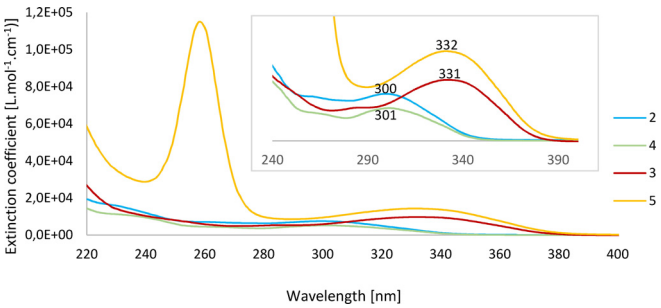

Figure 5. Solution UV spectra of siloles **2**–**5** in pentane or hexane.

bands for **3** and **5** therefore are likely a consequence of conjugation between the cross-hyperconjugated silole unit and the σ-conjugated oligosilane.

Computational results

DFT and TD-DFT analysis were performed on structures and electronic properties to investigate whether the bathochromic shift observed in the UV spectra for oligosilanyl substituted siloles **3** and **5** relative to those for silylated siloles **2** and **4** of approximatively $\Delta\lambda = 30$ nm arises indeed from conjugation of the extended oligosilane unit with the silole core. Computational details are given in the Supporting Information. Due to the size of silole **5** and since it shows very similar absorption characteristics to silole **3**, we excluded structure **5** from our theoretical study.

Since different functionals can produce diverse descriptions of these features, a DFT benchmark study was carried out using ten different functionals including dispersion and long-range corrections (B3LYP, B3LYP-D3, CAM-B3LYP, B97D, LC-wHPBE, M062X, M062X-D3, M06L, PBE0, w-B97XD) with the 6–311+G(d,p) basis set to determine the most accurate functional for the description of the synthesized siloles. With regard to structural properties, the optimized bond lengths (1–7 as shown in Figure 6) and the R-Si-C bond angle (α) are listed in Tables S2 and S3, respectively. Comparison with the X-ray diffraction data of the molecular structures of siloles **2**–**4** allows for a statistical evaluation of accuracy and reliability of the selected functionals by means of their mean unsigned errors (MUEs) (Figure S13). As for electronic properties, the first vertical excitations of target siloles computed using ten different TD-DFT functionals (Tables S4–S6) are compared with the experimental maximum absorbance. According to these assessments, the M062X functional reproduces very accurately the experimental molecular structures as obtained from XRD, and the major features observed experimentally in the absorption spectra of compounds **2**, **3** and **4**. For this reason, we refer here only to the computed data using the M062X functional.

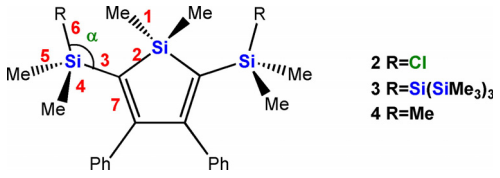

Figure 6. Representation of selected bonds and angles.

Structure

As structural indicators of both, σ- and π-conjugation, we have compared the lengths of the exocyclic Si–C single bonds and of the ring C=C double bonds as well as the R-Si-C angles of siloles **2**–**4** (Figure 6). Electron delocalization between the substituents in the 2,5-positions and the silole core generally leads to a shortening of single bonds and elongation of double bonds.[7] As it is shown in Table 2, change of the substituent R (as represented in Figure 6) in the 2,5-positions leads neither to elongation of the C=C double bond (7(C=C)) of the silole ring nor to a shortening of the exocyclic Si–C single bond (3 (Si–C)). However, the R-Si-C bond angle α calculated for tris-(trimethylsilyl)silyl-substituted silole **3** is widened from values typical for sp^3 hybridization of the carbon atom to values closer to sp^2 hybridization.

Table 2. Optimized bond lengths (pm) and bond angles α (°) for silyl substituted siloles (at M062X/6–311+G(d,p), experimental values in parenthesis).

Siloles	3 (Si–C)	7 (C=C)	α (R-Si-C)
2 (R = Cl)	185.7 (185.5)	135.3 (136.1)	104.3 (104.4)
3 (R = $Si(SiMe_3)_3$)	187.6 (187.0)	135.4 (136.0)	116.7 (118.3)
4 (R = Me)	187.5 (186.9)	135.3 (135.1)	106.6 (106.8)

The structural aspect of conjugation can be described by resonance structures that include no-bond-resonance structures (see Figure 7). We therefore performed an analysis based on natural resonance theory (NRT)[32] as implemented in the NBO 6 program in order to test the contribution of these no-bond-resonance structures for silyl substituted siloles **2**–**4** at the M062X/6–311+G(d,p) computational level. The results of this analysis are shown in detail in Figures S14–S16. The generated canonical structures in all cases represent 94–95% of the electronic structure. The chlorine- and the methyl-substituted siloles **2** and **4**, are very similar and the weight of the no-bond resonance structures **B** and **C** (Figure 7) that indicate hyperconjugation between the silyl group and the silole core is in both cases less than 4% (3.9% in **2** (R = Cl) and 3.7% in **4** (R = Me)). On the other hand, for silole **3** (R = $Si(SiMe_3)_3$), these no-bond-resonance structures have a notably higher contribution (7.7% in total), which implies that hyperconjugation between the silyl substituent and the silole core is more significant in silole **3**.

The computed NRT bond orders of silyl substituted siloles **2**–**4** derived from the contributing resonance structure are shown in Figure 8. As expected from the generated resonance

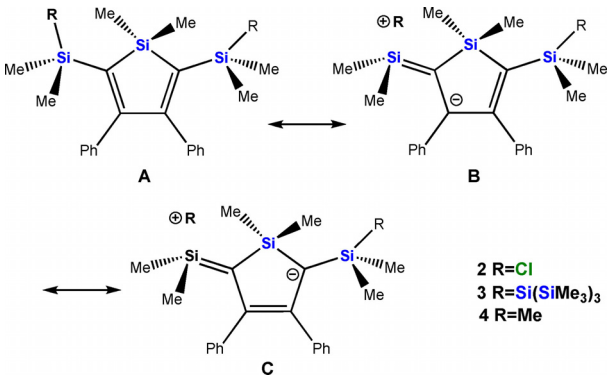

Figure 7. Plausible resonance structures **A**–**C** for silyl substituted siloles **2**–**4** including no-bond (R–Si) structures (**B**,**C**) that indicate hyperconjugation.

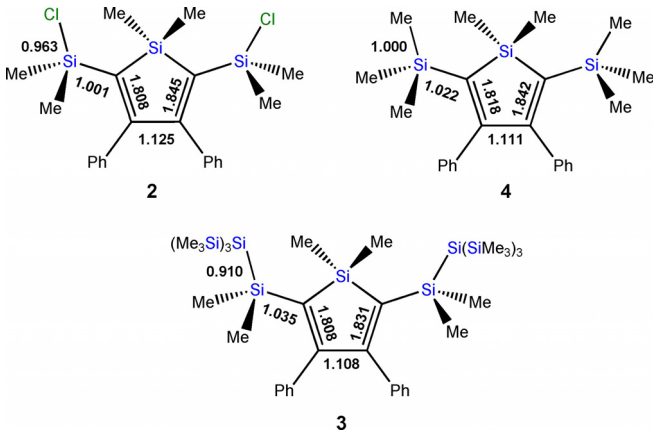

Figure 8. Calculated NRT bond orders of silyl substituted siloles **2**–**4** at the M062X/6–311+G(d,p) level.

structures by NRT analysis (Figures S14–S16), bond orders between 1.81 and 1.84 for the C=C double bonds and between 1.11–1.12 for the C–C single bond show the dominating butadiene-like delocalization on the silole rings in compounds **2**–**4**. In addition, when we compare the bond orders for the R–Si bonds, a gradual decrease in the bond orders according to the substituent order $Me > Cl > Si(SiMe_3)_3$ is apparent. Therefore, the results of our NRT analysis suggest an increasing importance of σ*(Si-R)-π(silole) hyperconjugation in oligosilanyl substituted siloles such as **3**. This is supported by visualization of the molecular orbitals (Figure 9) that show a marked contribution from Si–Si bonds to the HOMO of oligosilanyl substituted silole **3**, while no such contributions can be found for siloles **2** and **4**.

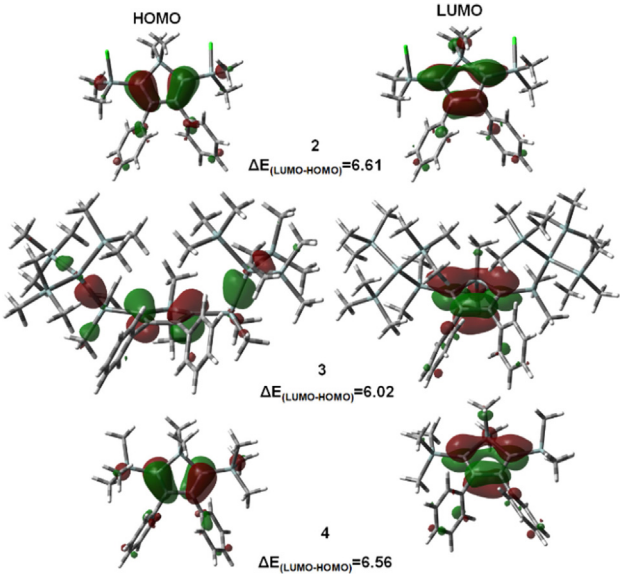

Figure 9. Molecular orbital diagrams of HOMO and LUMO for silyl substituted siloles **2**–**4**. (M062X/6–311+G(d,p) level, shown with an isodensity value of 0.04. HOMO/LUMO energy differences Δ*E* are given in eV).

TD-DFT results

The frontier orbital diagrams shown in Figure 9 suggest that the lowest energy transition for all three siloles is dominated by the π→π* transition of the silole core. Notably, the HOMO/LUMO energy difference Δ*E* is by 0.5 eV smaller for oligosilanyl substituted silole **3** than for siloles **2** and **4**, which is in qualitative agreement with the experimentally observed bathochromic shift. A closer inspection of the surface diagrams suggests that the HOMO of silole **3** is raised in energy due to the interaction of σ-Si–Si bonds of the silyl substituents with the highest occupied π-orbital of the butadiene part of the silole ring. For a quantitative comparison and a detailed analysis, we carried out time dependent DFT calculations (TD-DFT) for all three siloles **2**–**4** using their optimized molecular structures. The influence of hexane as a solvent on the transition energy was taken into account using the polarizable continuum model (PCM).[33] The characters of the first vertical excitations of target siloles are presented in Table 3 and the simulated UV spectra are depicted in Figure 10.

First, we note a pleasingly good agreement between the experimental λ_{max} values (Table 1, Figure 5) and the computed

Table 3. The computed (TD-M062X/6–311+G(d,p)) first vertical excitation energies [eV], corresponding wavelengths [nm] and oscillator strengths (*f*) for the siloles 2–4 in hexane. Substituent R as depicted in Figure 6.

Siloles	*E*	λ	*f*	Contribution
2 (R = Cl)	4.19	296.2 *300*	0.1425	HOMO- > LUMO (96%)
3 (R = $Si(SiMe_3)_3$)	3.76	329.5 *332*	0.2439	HOMO- > LUMO (77%), HOMO-7- > LUMO (6%), HOMO-6- > LUMO (2%), HOMO-4- > LUMO (4%), HOMO-2- > LUMO (4%)
4 (R = Me)	4.13	300.1 *301*	0.1292	HOMO- > LUMO (96%)

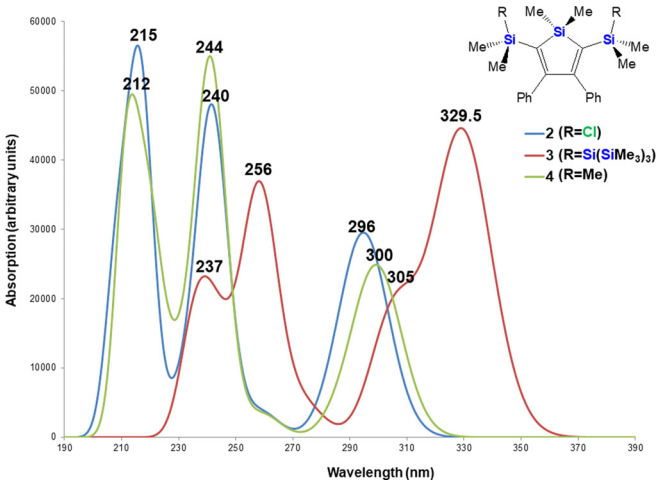

Figure 10. Simulated UV spectra of the siloles **2**–**4** (at TD-M062X/6–311+G(d,p) using PCM(hexane)).

transition energies (Table 3, Figure 10) for all three compounds. According to the TD-DFT analysis the low energy transition for siloles **2** and **4** (λ_{max}(calc) = 296 nm and 300 nm) are mainly contributed (96%) from HOMO to LUMO transitions. Regarding the oligosilanyl substituted silole **3**, the situation is more complicated. The contribution of the pure HOMO→LUMO transition is lower (77%) and other orbital transitions also have slight contributions to the first singlet transition (Table 3). In order to identify the nature of the first excitation of silole **3**, we additionally performed natural transition orbital[34] (NTO) analysis and some results are graphically depicted in Figure 11. For the chlorosilyl substituted silole **2**, the highest energy occupied and the lowest energy unoccupied orbitals are the 118th and 119th orbitals, respectively. The eigenvalues of those orbitals are 0.9912, so this excitation property is completely represented by these NTOs. A similar situation is encountered for the trimethylsilyl substituted silole **4**. As expected, the S0→S1 excitations for siloles **2** and **4** can (with a confidence of 99.1%) be regarded as transitions from occupied π orbitals to empty π*-orbitals of the silole rings (π→π* transition) (Figure 11) and there is no contribution from σ(Cl–Si) and σ(Me–Si) orbitals to NTOs for **2** and **4**, respectively.

Also in the case of oligosilanyl silole **3**, the S0→S1 transition is mainly (98.6%) consisting of a π→π* transition (from NTO 238 to NTO 239). It should be noted, however, that the σ(Si–Si) bond orbital additionally contributes to the NTO 238 (Figure 11), which is consistent with molecular orbital computations (Figure 9). Therefore, our computational analysis indicates extended conjugation between the oligosilanyl substituent and the silole core in silole **3**, which leads to the observed bathochromic shift of the π→π* transition by $\Delta\lambda_{max}$ = 30 nm compared to siloles **2** and **4**. The origin of the extended conjugation is effective σ*(SiSi)-π(silole) hyperconjugation in silole **3** as suggested by the canonical representations in Figure 7.

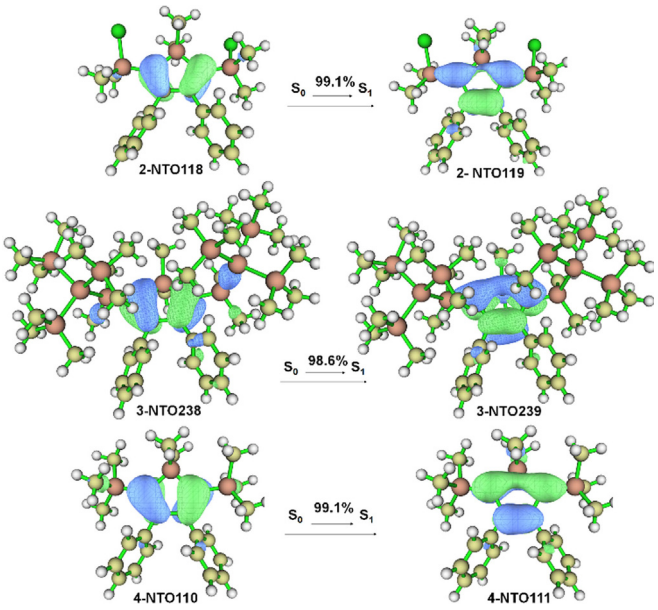

Figure 11. Graphical presentation of the NTO results for silyl substituted siloles **2**–**4**. (TD-M062X/6–311+G(d,p) (PCM, hexane), shown with an isodensity value of 0.04).

Stability of syn-Isomer

It is interesting that X-ray diffraction analysis of silole **3** revealed a *syn* orientation of both oligosilanyl substituents in 2- and 5-positions of the silole ring. Due to steric effects, we initially expected that *anti* orientation of these substituents would be more favored than *syn* orientation. Therefore, stability comparison for both conformations (Figure 12) was performed using M062X, B3LYP and B3LYP-D3 functionals with 6–311+G(d,p) basis set in both gas phase and hexane (Table 4). B3LYP and B3LYP-D3 functionals were used only to reflect the effect of dispersion correction on the computation of conformer stability. The results summarized in Table 4 indicate that the observed *syn*-conformation is more stable than the *anti*-conformation only when dispersion corrected B3LYP-D3 is used. This suggests that the conformation of the 2,5-oligosilanyl substituted silole **3** is determined by attractive London dispersion forces between the oligosilanyl groups. This is supported by the results of the M062X calculations which include dispersion forces by their parametrization and which predict an even stronger preference of the *syn*-conformation.

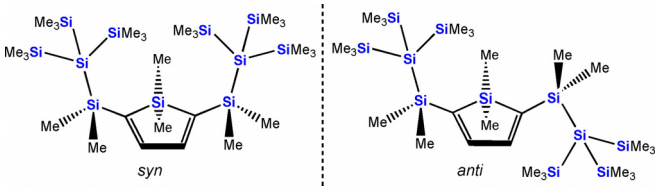

Figure 12. *Syn* (left) and *anti* (right) conformations of oligosilanyl substituted silole **3**.

Table 4. Relative energies (kJ mol^{-1}) of *syn*-**3** and *anti*-**3** in both gas phase and hexane (electronic energies including zero point vibrational energies are used).

	syn	*anti*
M062X/6–311+G(d,p)		
gas phase	0	20
hexane	0	19
B3LYP/6–311+G(d,p)		
gas phase	2	0
hexane	2	0
B3LYP-D3/6–311+G(d,p)		
gas phase	0	6
hexane	0	6

Conclusions

For the current account, we decided to study the combination of small oligosilanes with a silole ring. For this reason, we prepared a number of 2,5-disilylated 1,1-dimethyl-3,4-diphenylsiloles. One set of molecules (**2**, **4**) contained only monosilyl groups $SiMe_2Cl$ and $SiMe_3$ whereas oligosilanyl groups ($SiMe_2Si(SiMe_3)_3$ and $SiMe_2Si(SiMe_3)_2(SiMe_2)_2Si(SiMe_3)_3$) were attached to two other compounds (**3**, **5**). For both of the latter

cases a 30 nm bathochromic shift of the low energy absorption band, compared to the related compounds with either $SiMe_2Cl$ or $SiMe_3$ groups in 2,5-positions, was observed. This redshift of the absorption bands clearly suggests some type of conjugation between the silole and the oligosilane units. The hypothesis of conjugation between the oligosilane substituent and the silole core in compounds **3** and **5** was supported by the results of density functional computations. As indicated by NRT and NTO analysis, TD-DFT, and molecular orbital computations, the σ (Si–Si) bonds of the attached oligosilanyl fragments exhibit hyperconjugational interaction with the occupied π-orbitals of the butadiene part of the silole ring. This interaction between filled group orbitals leads to a higher energy of the HOMO and consequently to a smaller HOMO/LUMO energy difference. This results in the observed bathochromic shift of 2,5-bis(oligosilanyl) substituted siloles **3** and **5** compared to the bis(trimethylsilyl) substituted compound **4**.

It may be somewhat confusing to note almost identical absorption behavior for siloles **3** and **5** with attached linear trisilanyl and hexasilanyl units, respectively. This suggests that in both molecules the contributing oligosilanyl fragments must be similar. From previous studies on the UV/vis absorption properties of longer oligosilanes chains, it is known that for effective σ-conjugation a *transoid* conformation of the involved chain segment is required. A *cisoid* turn of the main chain leads to broken conjugation between the connected units.[30,31] For the cases of siloles **3** and **5**, we assume that only trisilanyl units fulfill the conformational demands of effective conjugation between the silole core and the oligosilanyl unit (cf. siloles **3** and **5** in Figure 13). For compound **5**, we assume that a *cisoid* turn separates the σ-conjugated hexasilane segment from interaction with the silole part (cf. silole **5** in Figure 13 with the hexasilane conjugation emphasized in orange on the left hand part and the trisilane-silole hyperconjugation (yellow-blue-green) for **3** and **5**). The conjugated hexasilane segment is responsible for the strong absorption band at 259 nm[30,31] in the absorption spectrum of **5** (Figure 5), whereas the band at 332 nm can be assigned to the HOMO/LUMO absorption due to hyperconjugation of the silole with the terminal trisilane segment.

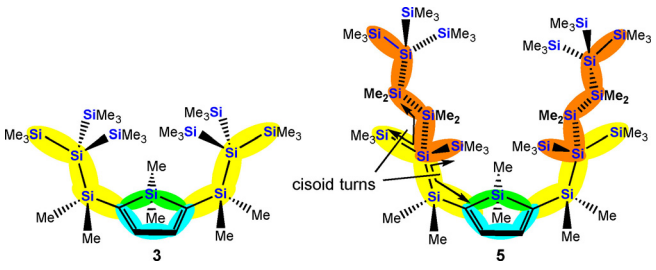

Figure 13. Spatial orientation of the oligosilane segments involved in different types of conjugation for siloles **3** and **5**. Hyperconjugational interaction between the silole and a trisilanyl unit shown for **3** and **5** (left and right) and isolated hexasilane σ-conjugation of **5** highlighted in orange.

Experimental Section

General remarks: All reactions involving air-sensitive compounds were carried out under an atmosphere of dry nitrogen or argon using either Schlenk techniques or a glove box. All solvents were dried using column based solvent purification system.[35] All used chemicals were obtained from different suppliers and used without further purification.

^1H (300 MHz), ^{13}C (75.4 MHz), and ^{29}Si (59.3 MHz) NMR spectra were recorded on a Varian INOVA 300 spectrometer. Spectra are referenced to tetramethylsilane (TMS) for ^1H, ^{13}C, and ^{29}Si. If not noted otherwise all samples were measured in C_6D_6. To compensate for the low isotopic abundance of ^{29}Si the INEPT pulse sequence was used for the amplification of the signal.[36,37] If the silole Si signal could not be observed this way, the Varian s2pul pulse sequence (gated-decoupling) was used. Elementary analyses were carried out using a Heraeus VARIO ELEMENTAR instrument.

X-ray structure determination: For X-ray structure analyses the crystals are mounted onto the tip of glass fibers, and data collection was performed with a BRUKER-AXS SMART APEX CCD diffractometer using graphite-monochromated Mo Kα radiation (0.71073 Å). The data were reduced to F^{2° and corrected for absorption effects with SAINT[38] and SADABS,[39,40] respectively. The structures were solved by direct methods and refined by full-matrix least-squares method (SHELXL97).[41] If not noted otherwise all non-hydrogen atoms were refined with anisotropic displacement parameters. All hydrogen atoms were located in calculated positions to correspond to standard bond lengths and angles. All diagrams are drawn with 30% probability thermal ellipsoids and all hydrogen atoms were omitted for clarity. Crystallographic data (excluding structure factors) for the structures of compounds **2**, **3**, and **4** reported in this paper are deposited with the Cambridge Crystallographic Data Center as supplementary publication no.

Deposition numbers 2011997, 2011995, and 2011996 (**2**, **3**, and **4**) contain the supplementary crystallographic data for this paper. These data are provided free of charge by the joint Cambridge Crystallographic Data Centre and Fachinformationszentrum Karlsruhe Access Structures service

Figures of solid state molecular structures were generated using Ortep-3 as implemented in WINGX[42] and rendered using POV-Ray 3.6.[43] Dimethylbis(phenylethynyl)silane (**1**),[44] tetrakis(trimethylsilyl)silane[45] and 1,1-dimethyl-3,4-diphenyl-2,5-bis(trimethylsilyl)silole (**4**)[46] were prepared following published procedures.

1,1-Dimethyl-2,5-bis(chlorodimethylsilyl)-3,4-diphenylsilole (2): To a solution of naphthalene (1.20 g, 4.7 equiv, 9.36 mmol) in THF (15 mL), small pieces of lithium ribbon (59 mg, 4.3 equiv, 8.50 mmol) were added and the malachite green solution was stirred for 3 h. Afterwards the solution was cooled to −90 °C and bis(alkynyl)silane **1** (522 mg, 1.0 equiv, 2.00 mmol) dissolved in THF (3 mL) was added dropwise within 1 min. Stirring was continued at −80 °C for 70 min and a dark brown color was observed. Then dichlorodimethylsilane (1.56 g, 6.0 equiv, 12.09 mmol) was added very fast and the solution was allowed to warm to rt after 15 min. The now pale yellow reaction mixture was stirred for 15 h after which volatiles were removed under reduced pressure. The residue was subjected to sublimation at 80 °C and 0.6 mbar to remove the majority of naphthalene (1.04 g, 87%). The remaining solid was extracted with pentane (2×10 mL). The yellow solution was kept at rt for crystallization. Compound **2** was obtained as colorless crystals (810 mg, 91%). Mp.: 133–134 °C. NMR (δ in ppm): ^1H: 6.93–6.73 (m, 10H), 0.73 (s, 6H), 0.18 (s, 12H). ^{13}C: 170.0, 145.0, 141.6, 128.7, 127.7, 127.3, 4.3, −2.7; ^{29}Si: 23.4 (s, silole-$SiMe_2$), 17.5 (s, $SiMe_2Cl$). Anal. calcd for $C_{22}H_{28}Cl_2Si_3$ (462.66): C 59.03, H 6.30.

Found: C 60.92, H 6.30. UV/vis: $\lambda_{max,1}$: 260.5 nm ($\varepsilon = 7.09 \times 10^3$ м$^{-1}$ cm^{-1}), $\lambda_{max,2}$: 300.0 nm ($\varepsilon = 7.52 \times 10^3$ м$^{-1}$ cm^{-1}).

1,1-Dimethyl-2,5-bis[tris(trimethylsilyl)silyldimethylsilyl]-3,4-diphenylsilole (3): Tetrakis(trimethylsilyl)silane (736 mg, 2.1 equiv, 2.29 mmol) and KO*t*Bu (272 mg, 2.2 equiv, 2.42 mmol) were dissolved in THF (3 mL) and were kept at rt for 18 h, until full conversion was detected (^{29}Si NMR). Volatiles were removed under reduced pressure and toluene (2 mL) was added to give an orange solution. This solution was added dropwise within 2 min to a solution of **2** (500 mg, 1.0 equiv, 1.12 mmol) in toluene (2 mL) and was stirred for 18 h at rt, after which full conversion was detected by NMR analysis. Solvents were removed to give a slightly yellow residue, which was extracted with pentane (4×4 mL), centrifuged and filtered. Colorless crystals (890 mg, 91%) of **3** were obtained from a pentane solution at −62 °C. Mp: 175–176 °C. NMR (δ in ppm): ^{1}H: 7.00–6.80 (m, 10H), 0.67 (s, 6H), 0.34 (s, 54H), 0.26 (s, 12H). ^{13}C: 169.3, 145.8, 143.2, 129.6, 127.5, 126.6, 5.9, 4.3, 0.5. ^{29}Si: 20.7 (s, silole-$SiMe_2$), −9.3 (s, $SiMe_3$), −19.0 (s, $SiMe_2$), −129.8 (s, Si_q). Anal. calcd for $C_{40}H_{82}Si_{11}$ (872.03): C 55.09, H 9.48. Found: C 54.88, H 9.49. UV/vis: $\lambda_{max,1}$: 286.0 nm ($\varepsilon = 5.29 \pm 0.05 \times 10^3$ м$^{-1}$ cm^{-1}), $\lambda_{max,2}$: 331.5 nm ($\varepsilon = 9.60 \pm 0.1 \times 10^3$ м$^{-1}$ cm^{-1}).

1,1-Dimethyl-2,5-bis[2′,2′,5′,5′,5′-pentakis(trimethylsilyl)-1′,1′,3′,3′,4′,4′-hexamethylpentasilanyl]-3,4-diphenylsilole (5): A solution of 2,2,5,5-tetrakis(trimethylsilyl)decamethylhexasilane (276 mg, 2.0 equiv, 0.45 mmol) and KO*t*Bu (53 mg, 2.1 equiv, 0.47 mmol) in THF (3 mL) was stirred at rt for 18 h, until full conversion was detected (^{29}Si NMR). Solvents were removed under reduced pressure to give a bright yellow residue, which was dissolved in toluene (2 mL). The silanide solution was added dropwise within 3 min to a solution of **2** (101 mg, 1.0 equiv, 0.23 mmol) in toluene (2 mL) and was stirred at rt for 24 h. The solvents were removed under reduced pressure and pentane (2×2 mL) was added. After centrifugation and filtration, pentane was removed in vacuo to give **5** (320 mg, 98%) as a yellow powder. Mp: 223–224 °C NMR: ^{1}H: 6.95–6.85 (m, 10H), 0.67 (s, 6H), 0.55 (s, 12H), 0.53 (s, 12H), 0.38 (s, 36H), 0.33 (s, 54+12H). ^{13}C: 169.8, 145.7, 143.1, 129.7, 127.5, 126.6, 6.8, 5.2, 4.0, 2.9, 2.1, 0.9. ^{29}Si: 20.9 (s, silole-$SiMe_2$), −9.2 [s, $Si(SiMe_3)_3$], −9.8 [s, $Si(SiMe_3)_2$], −18.4 (s, $SiMe_2$), −27.9 (s, $SiMe_2$), −28.6 (s, $SiMe_2$), −120.3 (s, Si_q), −128.0 (s, Si_q). UV/vis: $\lambda_{max,1}$: 259.0 nm ($\varepsilon = 116.0 \pm 1.0 \times 10^3$ м$^{-1}$ cm^{-1}), $\lambda_{max,2}$: 331.5 nm ($\varepsilon = 14.5 \pm 0.1 \times 10^3$ м$^{-1}$ cm^{-1}).

Acknowledgements

The authors would like to thank Prof. Karl Gatterer (TU Graz) for assistance with spectroscopic measurements. The Austrian part of this research was funded by the Austrian Science Fund (Fonds zur Förderung der wissenschaftlichen Forschung) (FWF) via project P-30955 (J.B.). In Oldenburg, support for this work was provided by the Deutsche Forschungsgemeinschaft (INST 184/108-1 FUGG). G.A.O. thanks The Philipp Schwartz Initiative of the Alexander Humboldt Foundation for financial support. The computations were carried out at the HPC Cluster, CARL, located at the University of Oldenburg (Germany) and funded by the DFG through its Major Research Instrumentation Program (INST 184/108-1 FUGG) and the Ministry of Science and Culture (MWK) of the Lower Saxony State. Open access funding enabled and organized by Projekt DEAL.

Conflict of interest

The authors declare no conflict of interest.

Keywords: cross hyperconjugation · oligosilanes · siloles · σ-conjugation

[1] R. S. Mulliken, *J. Chem. Phys.* **1939**, *7*, 339–352.
[2] R. S. Mulliken, C. A. Rieke, W. G. Brown, *J. Am. Chem. Soc.* **1941**, *63*, 41–56.
[3] S. Yamaguchi, K. Tamao, *J. Chem. Soc. Dalton Trans.* **1998**, 3693–3702.
[4] A. V. Denisova, R. Emanuelsson, H. Ottosson, *RSC Adv.* **2016**, *6*, 36961–36970.
[5] R. Emanuelsson, A. Wallner, E. A. M. Ng, J. R. Smith, D. Nauroozi, S. Ott, H. Ottosson, *Angew. Chem. Int. Ed.* **2013**, *52*, 983–987; *Angew. Chem.* **2013**, *125*, 1017–1021.
[6] R. Emanuelsson, H. Löfås, A. Wallner, D. Nauroozi, J. Baumgartner, C. Marschner, R. Ahuja, S. Ott, A. Grigoriev, H. Ottosson, *Chem. Eur. J.* **2014**, *20*, 9304–9311.
[7] A. V. Denisova, J. Tibbelin, R. Emanuelsson, H. Ottosson, *Molecules* **2017**, *22*, 370.
[8] A. Bande, J. Michl, *Chem. Eur. J.* **2009**, *15*, 8504–8517.
[9] H. Sakurai, M. Kumada, *Bull. Chem. Soc. Jpn.* **1964**, *37*, 1894–1895.
[10] H. Gilman, W. H. Atwell, G. L. Schwebke, *J. Organomet. Chem.* **1964**, *2*, 369–371.
[11] S. Yamaguchi, Y. Itami, K. Tamao, *Organometallics* **1998**, *17*, 4910–4916.
[12] S. Yamaguchi, T. Endo, M. Uchida, T. Izumizawa, K. Furukawa, K. Tamao, *Chem. Eur. J.* **2000**, *6*, 1683–1692.
[13] X. Zhan, S. Barlow, S. R. Marder, *Chem. Commun.* **2009**, 1948–1955.
[14] B. Z. Tang, X. Zhan, G. Yu, P. P. Sze Lee, Y. Liu, D. Zhu, *J. Mater. Chem.* **2001**, *11*, 2974–2978.
[15] J. Chen, C. C. W. Law, J. W. Y. Lam, Y. Dong, S. M. F. Lo, I. D. Williams, D. Zhu, B. Z. Tang, *Chem. Mater.* **2003**, *15*, 1535–1546.
[16] J. Mei, N. L. C. Leung, R. T. K. Kwok, J. W. Y. Lam, B. Z. Tang, *Chem. Rev.* **2015**, *115*, 11718–11940.
[17] S. Yamaguchi, K. Tamao, *Bull. Chem. Soc. Jpn.* **1996**, *69*, 2327–2334.
[18] K. Tamao, S. Yamaguchi, *J. Organomet. Chem.* **2000**, *611*, 5–11.
[19] H. Sohn, M. J. Sailor, D. Magde, W. C. Trogler, *J. Am. Chem. Soc.* **2003**, *125*, 3821–3830.
[20] M. Nakamura, Y. Ooyama, S. Hayakawa, M. Nishino, J. Ohshita, *Organometallics* **2016**, *35*, 2333–2338.
[21] T. Sanji, T. Sakai, C. Kabuto, H. Sakurai, *J. Am. Chem. Soc.* **1998**, *120*, 4552–4553.
[22] S. Yamaguchi, R.-Z. Jin, K. Tamao, M. Shiro, *Organometallics* **1997**, *16*, 2230–2232.
[23] K. W. Klinkhammer, W. Schwarz, *Z. Anorg. Allg. Chem.* **1993**, *619*, 1777–1789.
[24] C. Marschner, *Eur. J. Inorg. Chem.* **1998**, 221–226.
[25] C. Kayser, G. Kickelbick, C. Marschner, *Angew. Chem. Int. Ed.* **2002**, *41*, 989–992; *Angew. Chem.* **2002**, *114*, 1031–1034.
[26] J. Zhou, B. He, B. Chen, P. Lu, H. H. Y. Sung, I. D. Williams, A. Qin, H. Qiu, Z. Zhao, B. Z. Tang, *Dyes Pigm.* **2013**, *99*, 520–525.
[27] H. Okinoshima, K. Yamamoto, M. Kumada, *J. Am. Chem. Soc.* **1972**, *94*, 9263–9264.
[28] S. Yamaguchi, R.-Z. Jin, K. Tamao, M. Shiro, *Organometallics* **1997**, *16*, 2486–2488.
[29] H. Gilman, W. H. Atwell, P. K. Sen, C. L. Smith, *J. Organomet. Chem.* **1965**, *4*, 163–167.
[30] A. Wallner, H. Wagner, J. Baumgartner, C. Marschner, H. W. Rohm, M. Köckerling, C. Krempner, *Organometallics* **2008**, *27*, 5221–5229.
[31] J. Hlina, F. Stella, M. Aghazadeh Meshgi, C. Marschner, J. Baumgartner, *Molecules* **2016**, *21*, 1079.
[32] E. D. Glendening, F. Weinhold, *J. Comput. Chem.* **1998**, *19*, 610–627.
[33] S. Miertuš, E. Scrocco, J. Tomasi, *Chem. Phys.* **1981**, *55*, 117–129.
[34] R. L. Martin, *J. Chem. Phys.* **2003**, *118*, 4775–4777.
[35] A. B. Pangborn, M. A. Giardello, R. H. Grubbs, R. K. Rosen, F. J. Timmers, *Organometallics* **1996**, *15*, 1518–1520.
[36] G. A. Morris, R. Freeman, *J. Am. Chem. Soc.* **1979**, *101*, 760–762.

[37] B. J. Helmer, R. West, *Organometallics* **1982**, *1*, 877–879.
[38] A. Castel, P. Riviere, B. Saint-Roch, J. Satge, J. P. Malrieu, *J. Organomet. Chem.* **1983**, *247*, 149–160.
[39] R. H. Blessing, *Acta Crystallogr. Sect. A* **1995**, *51*, 33–38.
[40] G. M. Sheldrick, **2003**, SADABS. Version 2.10. Bruker AXS Inc., Madison, USA.
[41] G. M. Sheldrick, *Acta Crystallogr. Sect. C* **2015**, *71*, 3–8.
[42] L. J. Farrugia, *J. Appl. Crystallogr.* **2012**, *45*, 849–854.
[43] POVRAY 3.6. Persistence of Vision Pty. Ltd.: Williamstown, Victoria, Australia, **2004**. Available online: http://www.povray.org/download/, (accessed on 09.07.2008).
[44] Z. He, G. Lai, Z. Li, X. Yuan, Y. Shen, C. Wang, *Chin. J. Chem.* **2015**, *33*, 550–558.
[45] H. Gilman, C. L. Smith, *J. Organomet. Chem.* **1967**, *8*, 245–253.
[46] K. Tamao, S. Yamaguchi, M. Shiro, *J. Am. Chem. Soc.* **1994**, *116*, 11715–11722.

Manuscript received: July 2, 2020
Revised manuscript received: July 24, 2020
Accepted manuscript online: July 27, 2020
Version of record online: November 18, 2020

